Theoretical simulation of the barrier T2SLs InAs/InAsSb/B-AlSb longwave detector operating under thermoelectrical cooling

P. Martyniuk[1], K. Michalczewski[1], T.-Y. Tsai[2], C. H. Wu[2], Y. R. Wu[2]

[1] Institute of Applied Physics, Military University of Technology, 2 Urbanowicza Str., 00-908 Warsaw, Poland
(✉piotr.martyniuk@wat.edu.pl, +48 261839215)
[2] Graduate Institute of Photonics and Optoelectronics, National Taiwan University, Roosevelt Str., 10617 Taipei, Taiwan

***Abstract*–The paper reports on the barrier longwave infrared nBnn^{+} detector based on InAs/InAsSb (x_{Sb} = 0.38) type-II superlattice operating under thermoelectrical cooling (> 190 K). AlSb was proved to minimize barrier in valence band in analyzed temperature range and assumed architecture. The highest detectivity of the simulated structure was assessed at the level of ~ 10^{9} cmHz$^{1/2}$/W at T ~ 230 K assuming immersion contribution.**

I. Introduction

Infrared (IR) detectors operating in longwave range (LWIR) have many applications to include gas sensing being relevant for health condition monitoring and could be used in industry for the gas leak detection [1]. Sb based type-II superlattices (T2SLs) have been proposed as an alternative to the well known HgCdTe and T2SLs InAs/GaSb with lower fabrication cost and better performance with low dark current due to suppressed Auger generation-recombination (GR) rate and tunneling current [2]. The limiting factor of the widely studied T2SLs InAs/GaSb is the short minority carrier lifetime. That could be circumvented by “Ga-free” T2SLs InAs/InAsSb revealing very encouraging results in terms of carrier lifetime due to strong suppression of nonradiative recombination [3–5]. Expect material, it has been demonstrated that the simple barrier structures, e.g. nBn suppress the dark current through bandgap engineering [6]. A few papers have been published on HOT T2SLs detectors yet. Müller *et al.* showed T2SL InAs/GaSb immersed single pixel detector for LWIR with detectivity (D^{*}) = 3×10^{9} cmHz$^{1/2}$/W for ~9 µm 50 % cut-off [7]. The barrier nBn T2SLs InAs/InAsSb and InAs/GaSb detectors operating in cryogenic temperatures were reported by Teng *et al.* exhibiting D^{*} = 7.3×10^{11} cmHz$^{1/2}$/W for 8 µm 50 % cut off (InAs/GaSb), Kim *et al.* D^{*} = 10^{10} cmHz$^{1/2}$/W for 13.2 µm cut-off (InAs/InAsSb) and Haddadi *et al.* with D^{*} ~ 2×10^{11} cmHz$^{1/2}$/W for 9 µm (InAs/InAsSb) [8–10]. In this paper, we demonstrate theoretical modeling of LWIR nBnn^{+} barrier photodetector with T2SLs InAs/InAsSb (x_{Sb} = 0.38) active layer where AlSb barrier (B) was incorporated to provide nearly zero valence band offset (VBO) allowing unimpeded transport of the minority carriers (holes in terms of nBnn^{+} structure).

II. Simulation Procedure and Results

The nominal simulated LWIR T2SLs InAs/InAsSb/B-AlSb barrier structure is presented in Fig. 1. T2SLs InAs/InAsSb active layer (3 µm) and both contact layers (0.15 and 0.4 µm) were assumed to have 2.8 nm ($InAs_{0.62}Sb_{0.38}$) and 10.4 nm (InAs). The T2SLs InAs/InAsSb contact layers - 0.15 µm n-type, 10^{16} cm^{-3} and 0.4 µm n-type 5×10^{17} cm^{-3} and absorber - 3 µm, 10^{16} cm^{-3} were assumed.

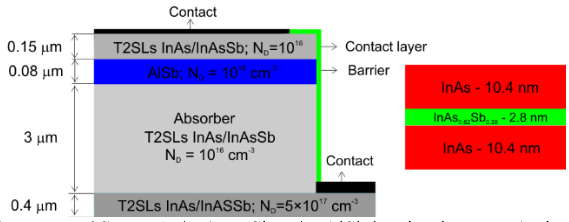

Fig. 1. LWIR T2SLs InAs/$InAs_{0.62}Sb_{0.38}$/B-AlSb barrier detector. Active layer – N_D =10^{16} cm^{-3}, barrier layer N_D = 10^{16} cm^{-3}, contact layers N_D = 5×10^{17} cm^{-3} and 10^{16} cm^{-3}.

The 80 nm, n-type 10^{16} cm^{-3} AlSb barrier was introduced to the detector’s structure.

Table 1. Material parameters assumed in modeling of LWIR T2SLs InAs/InAsSb.

Parameters	Symbols	GaAs	InAs	InSb	GaSb
Lattice constant a(T)=a(T=300K)+a_T×(T-300)	$a_T(Å/K)$	3.88×10^{-5}	2.74×10^{-5}	3.48×10^{-5}	4.72×10^{-5}
	a(T=300K)(Å)	5.65325	6.0583	6.4794	6.0959
Bandgap $E_g^{\Gamma}(T)= E_g^{\Gamma}(T{=}0K) - \frac{\alpha T^2}{T+\beta}$	α(meV/K)	0.5405	0.276	0.32	0.417
	β(K)	204	93	170	140
	E_g^{Γ}(T=0K) (eV)	1.519	0.417	0.25	0.812
Luttinger parameters	γ_1	7.05	20.0	34.8	13.4
	γ_2	2.35	8.5	15.5	4.7
	γ_3	3	9.2	16.5	6
Deformation potentials	a_c(eV)	-7.17	-5.08	-6.94	-7.5
	$a_v(eV)$	-1.16	-1	-0.36	-0.8
	b(eV)	-2	-1.8	-2	-2
	d(eV)	-4.8	-3.6	-4.7	-4.7
Elastic constant	C_{11}(GPa)	1221	832.9	684.7	884.2
	C_{12}(GPa)	566	452.6	373.5	402.6
	C_{44}(GPa)	600	395.9	311.1	432.2
Spin-orbit energy	Δ_0(eV)	0.341	0.39	0.82	0.76
Kane potential	E_p(eV)	23.81	21.5	24.08	24.76
Electron affinity	(eV)	4.07	4.9	4.59	4.06
Valence band offset	VBO(eV)	-0.8	-0.59	0	-0.03
Effective mass (0K)	$\frac{m_e^*}{m_0}$	0.064	0.023	0.0138	0.038

Table 2. Bowing parameters for InAsSb.

Bowing parameters	E_g^{Γ}(eV)	0.67
	Δ_0(eV)	1.2
	$m_e^*(\Gamma)$	0.035
	$E_{v,vac}$	-0.32, -0.4, -0.47

The 8×8 kp method was used to calculate bandgap energy and effective masses and carriers mobility in plane and growth directions. The material parameters assumed in T2SLs InAs/InAsSb modeling are presented in Table 1 and 2 [7]. The T2SLs InAs/InAsSb bandgap energy versus temperature and fitted Varshni equation are presented in Fig. 2 (a) while electron and hole effective masses are presented in Fig. 2 (b). Detector structure was simulated with software APSYS by Crosslight Inc. using bulk based model.

978-1-7281-1647-1/19/$31.00 ©2019 IEEE

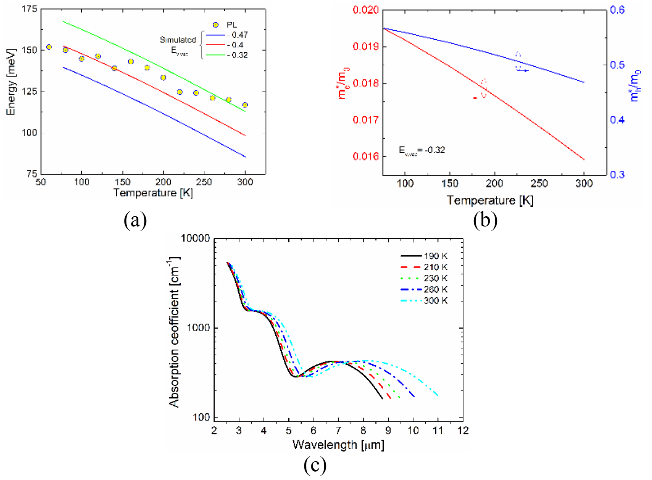

Fig. 2. T2SLs InAs/InAsSb bandgap energy simulated for selected $E_{v,vac}$ = -0.32, - 0.4, -0.47 (a) and electron/hole effective masses (b) versus temperature and absorption coefficient (c) versus wavelength and selected temperatures.

Calculated energy band diagram for nB_nnn^+ is presented in Fig. 3 for 230 K and 200 mV bias. Barrier in conduction band was estimated at the level of 1.5 eV.

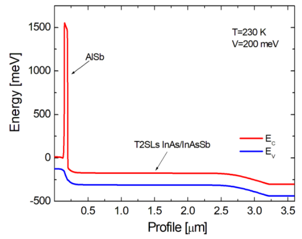

Fig. 3. Energy band diagram for LWIR T2SLs InAs/InAsSb/B-AlSb barrier $nBnn^+$ structure.

Dark current characteristic versus reciprocal temperature for nB_nnn^+ barrier structure for two selected voltages 50 mV and 200 mV is presented in Fig. 4 while photocurrent was shown in Fig. 5.

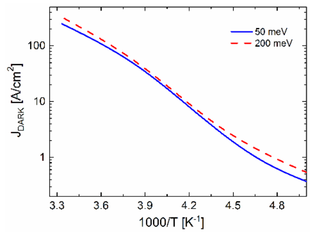

Fig. 4. Dark current for LWIR T2SLs InAs/InAsSb/B-AlSb barrier $nBnn^+$ structure for selected voltages 50 mV and 200 mV.

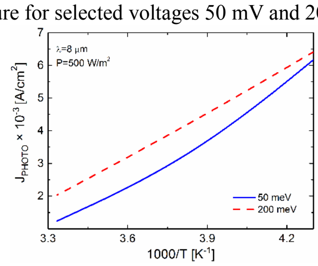

Fig. 5. Photocurrent for LWIR T2SLs InAs/InAsSb/B-AlSb barrier $nBnn^+$ structure for selected voltages 50 mV and 200 mV.

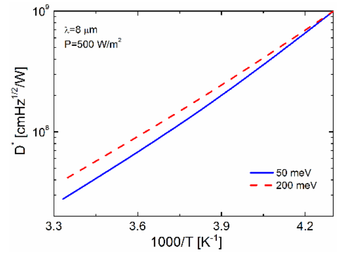

Fig. 6. Detectivity for LWIR T2SLs InAs/InAsSb/B-AlSb barrier $nBnn^+$ structure for selected voltages 50 mV and 200 mV.

III. Conclusions

We demonstrated theoretical modeling of LWIR $nBnn^+$ photodetectors with T2SLs InAs/InAsSb active layer where AlSb barrier was implemented. It was shown that material introduces nearly zero VBO in analyzed barrier structure. The highest D^* of the simulated structure was assessed at the level of ~ 10^9 cmHz$^{1/2}$/W at 230 K assuming immersion lens contribution.

Acknowledgment

This paper has been completed with the financial support of The National Centre for Research and Development-the grant no. PL-TW4/3/2017.

References

[1] Z. Bielecki, T. Stacewicz, J. Wojtas, J. Mikołajczyk, D. Szabra, A. Prokopiuk, “Selected optoelectronic sensors in medical applications”, Opto-Electronics Review 26(2), 122–133 (2018).
[2] D. Lackner, M. Steger, M. L. W. Thewalt, O. J. Pitts, Y. T. Cherng, S. P. Watkins, E. Plis, S. Krishna, “InAs/InAsSb strain balanced superlattices for optical detectors: Material properties and energy band simulations”, J. Appl. Phys. 111, 034507 (2012).
[3] T. Schuler-Sandy, S. Myers, B. Klein, N. Gautam, P. Ahirwar, Z.-B. Tian, T. Rotter, G. Balakrishnan, E. Plis, S. Krishna, “Gallium free type II $InAs/InAs_xSb_{1-x}$ superlattice photodetectors”, Appl. Phys. Lett. 101, 071111 (2012).
[4] E. H. Steenbergen, B. C. Connelly, G. D. Metcalfe, H. Shen, M. Wraback, D. Lubyshev, Y. Qiu, J. M. Fastenau, A. W. K. Liu, S. Elhamri, O. O. Cellek, Y.-H. Zhang, “Significantly improved minority carrier lifetime observed in a long-wavelength infrared III-V type-II superlattice comprised of InAs/InAsSb”, Appl. Phys. Lett. 99, 251110 (2011).
[5] L. Höglund, D. Z. Ting, A. Khoshakhlagh, A. Soibel, C. J. Hill, A. Fisher, S. Keo, S. D. Gunapala, “Influence of radiative and non-radiative recombination on the minority carrier lifetime in midwave infrared InAs/InAsSb superlattices”, Appl. Phys. Lett. 103, 221908 (2013).
[6] S. Maimon, G. W. Wicks, “nBn detector, an infrared detector with reduced dark current and higher operating temperature”, Appl. Phys. Lett. 89, 151109 (2006).
[7] R. Müller, V. Gramich, M. Wauro, J. Niemasz, L. Kirstea, V. Daumera, A. Janaszek, J. Jureńczyk, R. Rehm, “High operating temperature InAs/GaSb type-II superlattice detectors on GaAs substrate for the long wavelength infrared”, Infr. Phys. Tech., 96, 141–144 (2019).
[8] Y. Teng, Y. Zhao, Q. Wu, X. Li, X Hao, M. Xiong; Y. Huang, “High-performance long-wavelength InAs/GaSb superlattice detectors grown by MOCVD”, IEEE Photonics Technology Letters, 31, 185–188 (2018).
[9] H. S. Kim, O. O. Cellek, Zhi-Yuan Lin, Zhao-Yu He, Xin-Hao Zhao, Shi Liu, H. Li, and Y.-H. Zhang, “Long-wave infrared nBn photodetectors based on InAs/InAsSb type-II superlattices”, Appl. Phys. Lett. 101, 161114 (2012).
[10] A. Haddadi, G. Chen, R. Chevallier, A. M. Hoang, M. Razeghi, “$InAs/InAs_{1-x}Sb_x$ type-II superlattices for high performance long wavelength infrared detection”, Appl. Phys. Lett. 105, 121104 (2014).
[11] I. Vurgaftman, J. R. Meyer, “Band parameters for III–V compound semiconductors and their alloys”, J. Appl. Phys. 89, 5815 (2001).